Gas Phase Studies of Intermolecular Interactions and Relaxation

Cynthia J. Jameson

University of Illinois, Chicago, IL, USA

1 INTRODUCTION

The nuclear magnetic moment is a very sensitive site-specific probe of electronic environment and of dynamics in the gas, liquid, or solid phase. In this article, we specifically consider the nature of the information that can be obtained in the gas phase. Why should one do NMR spectroscopy in the gas phase? In the binary collision limit and in the zero-pressure limit, experimental measurements can be directly connected to quantities that can be calculated from first principles. Gas phase measurements therefore provide direct stringent tests of calculations of molecular electronic properties of the isolated molecule such as the rovibrationally averaged chemical shift, tests of intermolecular shielding surfaces and intermolecular potential surfaces from density and temperature dependence of chemical shifts in the binary collision limit, tests of relaxation theory near the T_1 minimum, and experimental values of cross sections for relaxation, which have a direct connection with the anisotropy of intermolecular potentials. Gas phase NMR measurements also provide cross sections for chemical reactions and intermolecular vibrational energy transfer, which are discussed in ***Gas Phase Studies of Chemical Exchange Processes***. The gas phase allows us to do experiments in theoretically tractable systems, then carry over the understanding to the less tractable condensed phase systems where possible.

Variable temperature studies can be carried out in the gas phase, where density is a variable that is independent of temperature. Equivalent experiments in the liquid phase would require high-pressure studies. The ability to work in a regime where only two-body effects are important permits the quantitative characterization of the observations with well-defined quantities such as the second virial coefficient of the chemical shift, which is a direct test of intermolecular shielding surfaces. The linear density region provides collision cross sections for molecular reorientation, or rotational angular momentum transfer, or intermolecular vibrational energy transfer leading to unimolecular reaction. These provide stringent tests of anisotropic intermolecular potentials, distinguishing between superficially similar potentials, and, in favorable cases, permitting refinement of the best available ones entirely on the basis of gas phase relaxation data. Furthermore, one can extrapolate the measured quantities to the zero-pressure limit to obtain the properties that are characteristic of the nearly isolated molecule, such as chemical shifts and coupling constants, which in turn can be related to intramolecular shielding and J coupling surfaces. At this limit, the intrinsic rate with which an energized molecule in the absence of collisions undergoes a unimolecular reaction such as ring inversion can also be obtained (see ***Gas Phase Studies of Chemical Exchange Processes***). A recent review of gas phase NMR studies spanning the density range $10^{16}-10^{21}$ molecules cm^{-3} and pressures from under 1 torr to 50 atm provides an overview, including experimental details.[1] In this article, we shall discuss only the intermolecular effects on chemical shifts, the temperature dependence of chemical shifts in nearly isolated molecules, and spin relaxation in the gas phase.

2 INTERMOLECULAR EFFECTS ON CHEMICAL SHIFTS

The nuclear magnetic shielding σ is determined by the electronic distribution around the nucleus of interest. Since interactions between molecules necessarily affect this distribution to some extent, there are observable effects of intermolecular interactions on σ. These intermolecular shifts can be rather large, and are usually observed as gas-to-liquid shifts or solvent shifts, which are difficult to describe quantitatively and interpret theoretically because they are dependent on the structure of the liquid. A table of gas-to-liquid shifts is given in ***Chemical Shift Scales on an Absolute Basis***. On the other hand, in a gas of modest density, the nuclear magnetic shielding σ, like other molecular electronic properties, can be expressed in terms of a virial expansion in density ρ:[2]

$$\sigma(T, \rho) = \sigma_0(T) + \sigma_1(T)\rho + \sigma_2(T)\rho^2 + \cdots \qquad (1)$$

Here, the terms dependent on the gas density ρ characterize the intermolecular effects, while the independent molecule value of the shielding, $\sigma_0(T)$, is a function of temperature owing to averaging over intramolecular motions (vibrations and rotations).[3] By analogy with the second virial coefficient in the usual expansion for PV/RT, $\sigma_1(T)$ may be called a second virial coefficient of the nuclear shielding. Both $\sigma_0(T)$ and $\sigma_1(T)$ can be obtained from experiments in the gas phase.[4] In a mixture of gases, $\sigma_1(T)$ due to A–A collisions and $\sigma_1(T)$ due to A–B collisions can be determined separately in a series of experiments. The sign of the intermolecular shielding effects has been found to be uniformly negative,[3,5]

$$[\sigma(T, \rho) - \sigma_0(T)] < 0 \qquad (2)$$

that is, intermolecular effects are deshielding, with only a few exceptions such as the nitrogen shielding in nitriles, pyridine and other similar nuclear sites involving n $\rightarrow \pi^*$ excited states.[6]

eMagRes, Online © 2007 John Wiley & Sons, Ltd.

This article was previously published in the *Encyclopedia of Magnetic Resonance* in 2007 by John Wiley & Sons, Ltd.
DOI: 10.1002/9780470034590.emrstm0185

2.1 Second Virial Coefficient of Nuclear Shielding

Operationally, $\sigma_1(T)$ is obtained as

$$\sigma_1(T) = -\frac{1}{\nu_0} \lim_{\rho \to 0} \left(\frac{\partial \nu}{\partial \rho} \right)_T \tag{3}$$

Since the gas phase measurements are not carried out on spherical samples, the measured $\sigma_1(T)$ have to be corrected for the bulk susceptibility, given to a good approximation by $\sigma_{1\text{bulk}} = \frac{2}{3}\pi\chi_{\text{mol}}$ or $-\frac{4}{3}\pi\chi_{\text{mol}}$ for the perpendicular or parallel arrangement of a cylindrical sample in the magnet, where χ_{mol} is the molar magnetic susceptibility of the sample. This is the same for all nuclei in the sample, and is a sizable fraction of the observed apparent $\sigma_1(T)$ for nuclei such as ^{1}H and ^{13}C, whereas it is a very small fraction for ^{129}Xe. Observed values of σ_1 range from -1×10^{-3} to about -1 ppm amagat^{-1} (1 amagat = 2.687×10^{25} molecules m^{-3}, the density of an ideal gas at 1 atm and 273.16 K). The range of values of σ_1 for a given nucleus not unexpectedly reflects the chemical shift range of the nucleus.[3] Xenon-129 in the Xe atom is found to be an ideal probe of intermolecular interactions. Xe intermolecular chemical shifts are very large in comparison with other nuclei.[7] After correction for bulk susceptibility, typical values of σ_1 at room temperature are[3,8,9] as shown in Table 1.

A summary of second virial coefficients of shielding for ^{19}F in various molecules has been given by Jameson.[1]

2.2 The Intermolecular Shielding Surface

For ^{129}Xe in dilute xenon gas, we can explicitly write $\sigma_1(T)$ in terms of the intermolecular potential function for Xe–Xe interactions and the nuclear shielding function for a Xe atom in a pair of interacting Xe atoms:

$$\sigma_1(T) = \int_0^\infty 4\pi r^2 \, \mathrm{d}r[\sigma(r) - \sigma(\infty)] \exp\left[-\frac{V(r)}{k_B T}\right] \tag{4}$$

where $\sigma(\infty)$ is the nuclear shielding of the isolated Xe atom and $\sigma(r)$ is the shielding of the Xe atom under the influence of a neighboring Xe atom at distance r from it. The expression applies to any pair of rare gas atoms, like or unlike.

A mean field long-range model for $[\sigma(r) - \sigma(\infty)]$ had been advanced by Raynes, Buckingham and Bernstein[10] (RBB) for a molecule in the presence of a neighbor at distance r and orientations given by θ_1, θ_2, ϕ_1, ϕ_2:

$$[\sigma(r, \theta_1, \theta_2, \phi_1, \phi_2) - \sigma(\infty)] = \sigma_a + \sigma_E + \sigma_W \tag{5}$$

They include a magnetic anisotropy term σ_a, electrical terms due to permanent electric moments on the neighbor σ_E, and a 'van der Waals term' σ_W, the intermolecular contributions to shielding due to dispersion, which was modeled by fluctuating electric fields produced at the molecule by mutual interactions with the neighbor in accordance with the London model of dispersion forces. The latter was taken to be of the form $-B\alpha_2 I_2 r^{-6}$, involving the polarizability and the ionization potential of the neighbor molecule and an empirical parameter B, which was taken to be the same as the average B in the quadratic response of the shielding in a molecule to a uniform static electric field. Later refinements involve the polarizability and ionization potential of the observed molecule as well, for example, $-3B\alpha_2 I_1 I_2 r^{-6}/2(I_1 + I_2)$. This is the only term in the model that applies to a pair of rare gas atoms. However, the magnitude of the average B that has been obtained by ab initio calculations[11] for ^{129}Xe in a Xe atom in a static uniform field when used in this model gives a value much too small to account for the observed $\sigma_1(T)$. Therefore, if the model is to be used in this form, the B parameter in it can no longer be identified with the average B in the shielding response to a uniform static electric field. Indeed, when the model is used, the empirical B parameter found in fitting the RBB equation, equation (5), to experiment is at least an order of magnitude larger, because this term in the model makes up for the shielding change due to overlap and exchange—terms that are missing in the long-range model, and which can only be obtained by ab initio calculations on the 'supermolecule' (the interacting pair of molecules).

Ab initio calculations of the intermolecular shielding function for ^{39}Ar in the argon atom interacting with another argon have revealed that dispersion contributions are not as important as was originally thought, and constitute only a minor correction when second-order correlation effects on shielding are included in the supermolecule calculation,[12] despite the nearly r^{-6} dependence of the shielding function in the region of interest (i.e., those values of r favored by the exp $[-V(r)/k_B T]$ weighting). Therefore, to the extent that ab initio shielding calculations at the level that includes second-order correlation effects are the basis for the inclusion of dispersion contributions, one may conclude that there are only very small contributions from dispersion in the intermolecular shifts of rare gases. The shape of the intermolecular shielding function for Ar–Ar is shown in Figure 1. This is the same shape as has been found for the shielding of ^{39}Ar in the Ar atom under the influence of Ne, and for ^{21}Ne shielding in the Ne atom in the presence of another Ne atom or a He atom.[13] It has been found that when this shielding function is scaled up to ^{129}Xe in various Xe–rare gas pairs, it is possible to reproduce quantitatively the $\sigma_1(T)$ observed for ^{129}Xe in pure xenon, and also for Xe with Kr and for Xe with Ar, in their signs, magnitudes, and temperature dependences.[12] The relative magnitudes of the temperature dependences in these three systems are also reproduced.

Table 1 Second Virial Coefficients of Nuclear Shielding

	$-\sigma_1$(ppm amagat^{-1})
^{1}H	0.0003–0.008
^{11}B	0.0085 (in BF_3)
^{13}C	0.0022–0.0105
^{15}N	0.0026–0.04
^{19}F	0.006–0.05
^{31}P	0.0023–0.266
^{77}Se	0.007 (in SeF_6)
^{83}Kr	0.131
^{125}Te	0.01 (in TeF_6)
^{129}Xe	0.166–0.75

eMagRes, Online © 2007 John Wiley & Sons, Ltd.

This article was previously published in the *Encyclopedia of Magnetic Resonance* in 2007 by John Wiley & Sons, Ltd.
DOI: 10.1002/9780470034590.emrstm0185

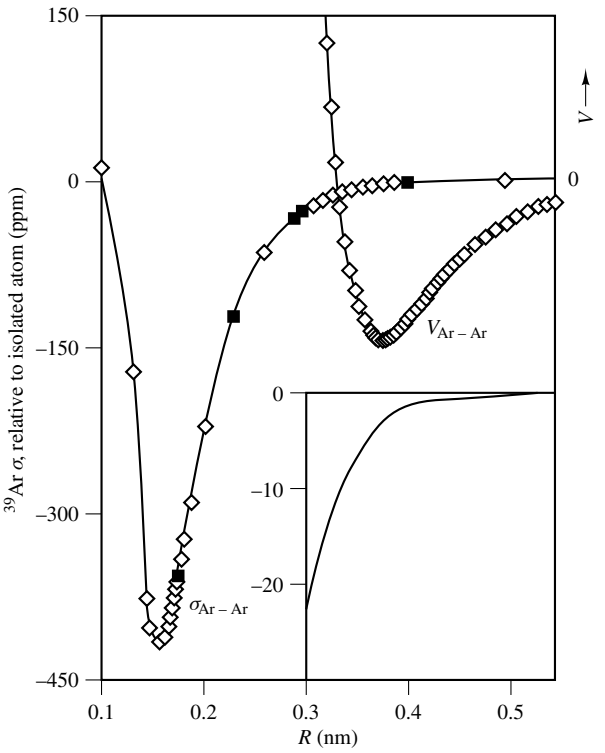

Figure 1 Intermolecular shielding function for ^{39}Ar in Ar–Ar obtained from ab initio calculations. Adapted from Jameson and de Dios[12] by permission. The values denoted by ■ include second-order correlation contributions, all other values are from a coupled Hartree–Fock calculation, using the local origins method described in the article ***Chemical Shift Calculations by the LORG & SOLO Approaches***

2.3 The Nuclear Site Effect

Intermolecular shieldings are different for different nuclear sites in a molecule under the influence of a solvent molecule. In averaging over all the orientations of the molecule bearing the observed nuclei, the peripheral nuclei suffer larger intermolecular effects than nuclei located in the interior. That is why relatively protected nuclei such as ^{77}Se in SeF_6 or ^{125}Te in TeF_6 have fairly small intermolecular shifts compared with ^{77}Se in H_2Se or ^{125}Te in H_2Te. A direct comparison is possible when the nuclei are the same type and in the same molecule, such as the two N nuclei in the NNO molecule or the three different ^{19}F nuclei in $F_2C{=}CFH$. A simple model by Rummens et al.[14] depends on the averaging of r_{NS}^{-6} distances between nucleus N and solvent S, while the isotropic intermolecular potential is expressed in terms of the separation R_{CS} between the center of mass of the molecule and the solvent. The average intermolecular shift can then be expressed in terms of the distance d between the nuclear site and the center of mass of the molecule. The distance d changes systematically for each of the three types of F nuclear sites in $F_2C{=}CFX$, where X varies as H, F, Cl, Br, and I. It has been demonstrated that in this series of molecules, this model provides semiquantitative agreement with experiment in the pure gases; the $\sigma_1(T)$ for the three different ^{19}F nuclei vary with the respective values of d for the nuclear site as expected.[15] Similarly, in the NNO molecule, the end nitrogen nucleus has a larger intermolecular shift in pure NNO, and in NNO–rare gas, and NNO–SF_6 mixtures.

2.4 Intermolecular Contact Shifts

The ^{129}Xe chemical shifts for Xe in the paramagnetic gases O_2 and NO exhibit a linear dependence on the density of O_2 (or NO) with unusually large slopes.[16,17] There is, of course, the bulk susceptibility contribution to the apparent $\sigma_1(T)$, but this can easily be corrected for, using

$$\chi_{mol} = N_{Avo}\langle\mu_{eff}^2\rangle/3k_BT \tag{6}$$

where $\langle\mu_{eff}^2\rangle$ is a very nearly temperature-independent 8 Bohr magnetons for O_2 and a strongly temperature dependent average value for NO. In addition to this bulk susceptibility contribution, there is a strongly temperature-dependent true $\sigma_1(T)$, which has a very different behavior from that in the ^{129}Xe $\sigma_1(T)$ for Xe in Ar, for example. This $\sigma_1(T)$ includes, in addition to the usual intermolecular shielding contribution, a contact shift that arises from the finite electron spin density ρ_{spin} at the ^{129}Xe nucleus from the interaction of the Xe with O_2 or NO, which Buckingham and Kollman[18] attributed to the overlap of the $O_2(\pi_g{}^*)$ or NO(π^*) orbitals with the Xe(5s). That is,

$$\sigma_1(\text{contact}) = -\frac{4}{3}\pi\frac{\langle\mu_{eff}^2\rangle}{3k_BT}\int_0^\infty 4\pi r^2\,dr\rho_{spin}\exp\left[-\frac{V(r)}{k_BT}\right] \tag{7}$$

It was found that if the normal ^{129}Xe $\sigma_1(T)$ for Xe in hypothetically diamagnetic O_2 or NO were taken to be the same as the observed ^{129}Xe $\sigma_1(T)$ for Xe in Ar and the distance dependence of the shielding change due to contact shift were similar to that of the $\sigma(r)$ for ^{129}Xe in Ar, then the limiting temperature dependence of the contact shift could be extracted. The latter is found to be $1/T$ at the lower temperatures, just as the Curie law behavior predicts, and the magnitude of the intermolecular contact shielding is roughly three times that of the ^{129}Xe $\sigma(r)$ for Xe in Ar. The integrals shown above can be extracted empirically from the observed density and temperature dependence of the shifts, and are found to have a ratio 1.25 for NO/O_2, which agrees with the ratio calculated by Buckingham and Kollman.

2.5 Many Body Terms

The dependence on density becomes nonlinear as the densities approach liquid densities.[19] The intermolecular shielding contributions from the many body terms are found to be opposite in sign to the two-body second virial coefficient of shielding that is found in the dilute gas.[1] That is, the effective density coefficient of shielding for liquids is smaller in magnitude than the σ_1 obtained in the dilute gas. Both are deshielding (excepting the cases of nitrile or pyridine nitrogen nuclei already mentioned), but liquids are less deshielded than one might expect from direct extrapolation to liquid densities. The gas-to-liquid shift thus gives an estimate of σ_1 that is somewhat too small in magnitude, but nevertheless provides a reasonable estimate of σ_1 when density dependence measurements cannot be carried out. The general shape of ab initio intermolecular shielding surfaces and assumption of

eMagRes, Online © 2007 John Wiley & Sons, Ltd.

This article was previously published in the *Encyclopedia of Magnetic Resonance* in 2007 by John Wiley & Sons, Ltd.
DOI: 10.1002/9780470034590.emrstm0185

largely pairwise-additive shielding contributions are found to be consistent with the signs and general magnitudes of gas-to-liquid and gas-to-solution shifts and adsorption shifts.[20] A favorable example is the set of chemical shifts and their temperature dependence in Xe, Xe_2, Xe_3, ... , Xe_8 clusters trapped in zeolite NaA, which have been reproduced by using grand canonical Monte Carlo averaging of ^{129}Xe shieldings assuming pairwise additive isotropic shieldings based on ab initio shielding functions in rare gas pairs.[21]

3 TEMPERATURE DEPENDENCE OF NUCLEAR SHIELDING IN THE ISOLATED MOLECULE

After extrapolation to zero density, there should be no remaining temperature dependence in the case of xenon. However, it was discovered during measurements of σ_1 that the zero-density intercept of the chemical shift changed with temperature when the molecule bearing the nucleus had internal degrees of freedom, and dramatically so for ^{19}F nuclei.[4] In practice, the temperature dependence in the limit of zero density is not obtained from the intercepts; rather, the $\sigma_1(T)$ function is fully characterized experimentally from the density dependence of the chemical shift in several samples and then $\sigma_1(T)\rho$ is subtracted from every data point to correct each to the zero-density limit, thereby obtaining $[\sigma_0(T) - \sigma_0(300\,\mathrm{K})]$. The general shape of these functions is that the nucleus becomes more deshielded with increasing temperature, usually with a nonlinear temperature dependence, although in the cases of ^{13}C in CO and ^{15}N in N_2 the function is a linear one.[22] The magnitude of the temperature coefficient depends on the nucleus—larger for ^{31}P and ^{19}F than for ^{13}C. Some examples are shown in Table 2. There is some evidence that the temperature coefficient is very large for transition metal nuclei, although these have been studied in solution rather than in the limit of zero-density gas. For a given nucleus, the temperature coefficient correlates with the shielding, and is larger for less shielded environments.

The temperature dependence of the shielding results from the same rotational and vibrational averaging that is responsible for isotope shifts. In the context of the Born–Oppenheimer approximation, the separation of the electronic from the nuclear motion allows an intramolecular potential surface to be defined, which is then used in finding the vibrational states and functions. In the same context, the nuclear shielding surface is defined: this is a mathematical surface containing the values of the shielding as a function of the positions of the nuclei in the molecule. Some examples of shielding surfaces are given in ***Isotope Effects on Chemical Shifts and Coupling Constants***. The entire shielding tensor changes with the molecular internal geometry, but only the isotropic average about all orientations of the molecule with respect to the external magnetic field concerns us in the gas phase. Thus, the isotropic shielding surface can be described in terms of an expansion of the shielding in powers of the nuclear displacement coordinates such as bond stretches and bond angle deformations and the derivatives of the shielding with respect to these stretches and deformations:

$$\begin{aligned}\sigma(\mathrm{F}_1) = \sigma_\mathrm{e} &+ \left(\frac{\partial\sigma}{\partial r_1}\right)_\mathrm{e}\Delta r_1 + \left(\frac{\partial\sigma}{\partial r_2}\right)_\mathrm{e}\Delta r_2 \\ &+ \sum_{i=3}^{6}\left(\frac{\partial\sigma}{\partial r_i}\right)_\mathrm{e}\Delta r_i + \left(\frac{\partial^2\sigma}{\partial r_1^2}\right)_\mathrm{e}(\Delta r_1)^2 + \left(\frac{\partial^2\sigma}{\partial r_2^2}\right)_\mathrm{e}(\Delta r_2)^2 \\ &+ \sum_{i=3}^{6}\left(\frac{\partial^2\sigma}{\partial r_i^2}\right)_\mathrm{e}(\Delta r_i)^2 + \left(\frac{\partial^2\sigma}{\partial\alpha_{12}\partial r_1}\right)_\mathrm{e}\Delta r_1\Delta\alpha_{12} + \cdots \end{aligned} \quad (8)$$

for ^{19}F in an MF_6 molecule, for example. The thermal average of σ then gives $\sigma_0(T)$. The thermal averages of the nuclear displacement coordinates can be obtained if the intramolecular force field is available, as they are for SF_6, for example. In ***Isotope Effects on Chemical Shifts and Coupling Constants***, it is shown how these averages are

Table 2 Temperature Coefficients of the Shielding for Molecules in the Zero-Pressure Limit at 300 K

	Molecule	$d\sigma_0(T)/dT$ (ppb K^{-1})		Molecule	$d\sigma_0(T)/dT$ (ppb K^{-1})
^{13}C	CH_4	−0	^{15}N	N_2	−0.85
	CO	−0.29		NNO	−3.5, −8.8
	CO_2	−0.54	^{19}F	BF_3	−1.33
^{19}F	SiF_4	−3.81		$CFCl_3$	−11.6
	CF_4	−5.01		CF_2HCl	−4.86
	POF_3	−5.65		$CFHCl_2$	−5.92
	PF_3	−6.73		CF_3CH_3	−10.3
	PF_5	−9.79		CF_2HCH_3	−10.8
	ClF	−10.4		CF_3CF_3	−11.4
	SF_6	−12.1		CF_3CF_2Cl	−11.3
	TeF_6	−16.1		CF_2ClCF_3	−13.1
	SeF_6	−22.9		OCF_2	−4.33
	WF_6	−23.3		$CF_2{=}CH_2$	−4.07
	NF_3	−20.0		$CF_2{=}CF_2$	−8.13
	F_2	−34.0		$CF_2{=}CFH$	−5.06, −5.11, −6.76
	CH_3F	−1.76		$CF_2{=}CFCl$	−7.87, −8.73, −10.6
	CH_2F_2	−2.89		$CF_2{=}CFBr$	−8.04, −9.07, −11.5
	CF_3H	−5.60		$CF_2{=}CFI$	−6.98, −8.77, −12.8
	CF_3CN	−7.57	^{31}P	PH_3	−0.5
	CF_3I	−9.25		PF_3	−1.7
	CF_3Br	−10.2		POF_3	−1.4
	CF_3Cl	−6.78	^{77}Se	SeF_6	−14
	CF_2Cl_2	−9.06	^{125}Te	TeF_6	−10

eMagRes, Online © 2007 John Wiley & Sons, Ltd.

This article was previously published in the *Encyclopedia of Magnetic Resonance* in 2007 by John Wiley & Sons, Ltd.
DOI: 10.1002/9780470034590.emrstm0185

obtained in general. Given the ab initio surface, or the shielding derivatives, and the intramolecular force field, the $\sigma_0(T)$ can be calculated and compared with experiment. It is generally not possible to obtain accurate derivatives of shielding directly from the experimentally observed $\sigma_0(T) - \sigma_0(300\,\mathrm{K})$ functions even using very accurate force fields, since the nature of the experimental data allows typically only one, at most two, parameters to be determined empirically. The empirical shielding derivatives that have been estimated from the temperature dependence of the shielding of ^{19}F have made use of the assumption that the bond extension terms completely dominate the shielding. In this way, estimates of the shielding derivatives in the fluoromethanes, fluoroethenes, and MF_6 type molecules have been made. The observed temperature coefficients $d\sigma_0(T)/dT$ for a series of related compounds such as for ^{19}F in substituted fluoromethanes, and generally for ^{19}F in binary fluorides, correlate with the ^{19}F chemical shifts in these compounds, and the least shielded environments show the largest temperature coefficients. The correlation is even better with the paramagnetic part of the shielding.[9] Although the derivatives in these particular molecules have not been provided by ab initio calculations, it has been found that, for a large number of molecules, the ab initio shielding derivatives for ^{19}F generally correlate with the shielding itself.[20,23] In the case of F_2, the shielding derivative estimated from the temperature dependence appears to be too large compared with the ab initio calculations. In N_2 and CO, the shielding first derivatives estimated from the temperature dependences of the ^{15}N and ^{13}C nuclei, respectively, are roughly the same as those calculated from the ab initio surfaces for these molecules.

4 SPIN RELAXATION IN THE GAS PHASE

Spin relaxation in the gas phase provides qualitatively different information from that in the liquid phase. Since the intermolecular dynamics in the gas phase can be modeled more accurately, the gas phase provides critical tests of relaxation theories, allows quantitative separation of two or more contributing mechanisms, and provides a direct connection with the anisotropy of intermolecular potentials.

4.1 Theoretical Treatments of Relaxation and the Connection with Intermolecular Potentials

NMR studies of spin relaxation in molecular gases provide a very sensitive probe of the anisotropic part of the intermolecular potential surfaces. As a function of gas density ρ, the spin–lattice relaxation time T_1 is long at low densities, for which the collision frequency is very low, passes through a characteristic minimum corresponding to a matching between the collision and spin precession frequencies, and then passes into a regime in which it increases linearly with gas density, the so-called 'extreme narrowing' regime. As the density increases, there is a less efficient communication through the weak intermolecular coupling between the rotational degrees of freedom (the 'lattice') and the nuclear spin system of the effects of reorienting molecular collisions to the nuclear spins. The region of the T_1 minimum permits a measurement of the strength of the interaction that couples the nuclear spin system to the lattice degrees of freedom. Bloch's phenomenological equations (***Relaxation: An Introduction***) provide a description of nuclear magnetic relaxation in gas phase systems. In order to make the connection with intermolecular potential energy surfaces, it is necessary to express the relaxation times T_1 and T_2 in Bloch's equations in terms of quantities that may be directly calculated once an intermolecular potential energy surface has been specified. There are several approaches: the traditional one is to apply correlation function theory to a master equation. This is the approach used by Abragam[24] and by Bloom and Oppenheim.[25,26] Another approach is to employ the kinetic theory of gases in the context of a generalized Boltzmann equation.[27] It has been demonstrated by McCourt et al.[28,29] that the most useful features of each method can be retained in a unified theory by utilizing a projection operator formalism to obtain a memory equation for that part of the distribution function density matrix characterizing the gaseous system and proportional to the nuclear spin operator $\hat{\boldsymbol{I}}$. The memory equation thus obtained is utilized to obtain an integral equation governing the time dependence of the nonequilibrium part of the nuclear magnetization in terms of a kernel having the form of an autocorrelation function.

In the single relaxation time approximation (SRTA), a common correlation time is assumed for all the rotational levels. A multiple relaxation time approximation (MRTA) uses a distribution of correlation times, and has been shown to be necessary in the accurate analysis of the proton relaxation in HCl and in NH_3 molecules in the range of densities including the T_1 minimum, which then provides spin rotation tensor elements that are in excellent agreement with molecular beam values.[30] General multilevel expressions for the contributions to the nuclear magnetic relaxation from spin rotation, dipolar, intramolecular, and quadrupolar mechanisms have been given independently by Gordon[31,32] and by McCourt[29] which we shall illustrate here using the example of the D_2 molecule, since it includes three major relaxation mechanisms: spin–rotation, intramolecular dipolar, and quadrupolar mechanisms.

The relaxation of nuclei of rare gas atoms is strictly intermolecular.[33] Although both intermolecular and intramolecular relaxation mechanisms contribute in general to the relaxation of nuclei in molecular gases, intramolecular relaxation dominates by five or so orders of magnitude (excepting the intermolecular relaxation due to a paramagnetic collision partner, which we shall consider later). It is also typical of the molecular gases that have been studied that shielding anisotropy and scalar coupling mechanisms are not important. We shall also only show here the theoretical expressions (following McCourt[29,34,35]) appropriate to the *linear density regime* (extreme narrowing conditions), which provide the connection with the anisotropy of intermolecular potential surfaces. This regime is characterized by T_1/ρ. In H_2, only the spin rotation and dipolar mechanisms, and in D_2, spin–rotation, dipolar and quadrupolar mechanisms have to be considered. For H_2, only the *ortho* modification has a nonzero total nuclear spin, whereas in D_2, *para* and *ortho* modifications have to be considered separately:

$$\left(\frac{\rho}{T_1}\right)_{\mathrm{lin}} = \left(\frac{\rho}{T_1}\right)_{\mathrm{lin,sr}} + \left(\frac{\rho}{T_1}\right)_{\mathrm{lin,dq}} \tag{9}$$

The expressions for H_2(*ortho*) are

$$\frac{\rho}{T_1} \qquad = \frac{2}{3}\frac{(\omega_{\mathrm{sr}}^{\mathrm{H}})^2}{L_0\ \mathrm{v}}\,\boldsymbol{d}^{(1)\mathrm{T}} \cdot \langle \boldsymbol{\sigma}_{\mathrm{v}} \rangle^{-1} \cdot \boldsymbol{P} \cdot \boldsymbol{d}^{(1)} \tag{10}$$

eMagRes, Online © 2007 John Wiley & Sons, Ltd.

This article was previously published in the *Encyclopedia of Magnetic Resonance* in 2007 by John Wiley & Sons, Ltd.
DOI: 10.1002/9780470034590.emrstm0185

$$\left(\frac{\rho}{T_1}\right)_{\text{lin,d}} = \frac{(\omega_{\text{d}}^{\text{H}})^2}{L_0\langle \text{v}\rangle}\, \boldsymbol{d}^{(2)\text{T}} \cdot \langle \boldsymbol{\sigma}_{\text{T}}\rangle^{-1} \cdot \boldsymbol{P} \cdot \boldsymbol{d}^{(2)} \tag{11}$$

whereas for the D_2 molecule,

$$\left(\frac{\rho}{T_1}\right)_{\text{lin,sr}} = \frac{2}{3}\frac{(\omega_{\text{sr}}^{\text{D}})^2}{L_0\langle \text{v}\rangle}\, \boldsymbol{d}^{(1)\text{T}} \cdot \langle \boldsymbol{\sigma}_{\text{v}}\rangle^{-1} \cdot \boldsymbol{P} \cdot \boldsymbol{d}^{(1)} \tag{12}$$

$$\left(\frac{\rho}{T_1}\right)_{\text{lin,dq}} = \frac{(\omega_{\text{dq}}^{\text{D}})^2}{L_0\langle \text{v}\rangle}\, \boldsymbol{d}^{(2)\text{T}} \cdot \langle \boldsymbol{\sigma}_{\text{T}}\rangle^{-1} \cdot \boldsymbol{P} \cdot \boldsymbol{d}^{(2)} \tag{13}$$

The gas density ρ is measured in amagats, $L_0 = 2.687 \times 10^{25}$ molecules m^{-3}, the number density corresponding to 1 amagat, $\langle \text{v}\rangle$ is the mean relative velocity $(8k_{\text{B}}T/\pi\mu)^{1/2}$, with μ the reduced mass of the colliding pair. The other quantities are described below. The intramolecular spin–rotation and dipolar frequencies come from the intramolecular interaction Hamiltonian in terms of first- and second-rank irreducible tensors:

$$\hat{\mathcal{H}} = -\hbar\omega_{\text{sr}}^{\text{D}}\hat{\boldsymbol{I}}\cdot\hat{\boldsymbol{J}} + \hbar\omega_{\text{d}}^{\text{D}}\overline{\boldsymbol{I}_1\boldsymbol{I}_2}:\overline{\boldsymbol{u}\boldsymbol{u}} - \hbar\omega_{\text{d}}^{\text{D}}(\overline{\boldsymbol{I}_1\boldsymbol{I}_1} + \overline{\boldsymbol{I}_2\boldsymbol{I}_2}):\overline{\boldsymbol{u}\boldsymbol{u}} \tag{14}$$

The off-diagonal matrix elements of $\overline{\boldsymbol{u}\boldsymbol{u}}$ lead to high-frequency effects in NMR,[26,29,36] which will only affect the NMR relaxation process at densities in which the collision frequencies are comparable to any of the rotational frequencies, at which densities the O and S branches of the Raman spectrum are sufficiently collisionally broadened to overlap with the Q branch. This is usually the case in liquids. For H_2, such an overlap does not occur even up to densities of 1000 amagat. For dilute gases, the high-frequency terms arising from the off-diagonal matrix elements of $\overline{\boldsymbol{u}\boldsymbol{u}}$ do not play a significant role in the relaxation; thus, only the diagonal part of $\overline{\boldsymbol{u}\boldsymbol{u}}$ is taken into account:

$$\hat{\mathcal{H}} = -\hbar\omega_{\text{sr}}^{\text{D}}\hat{\boldsymbol{I}}\cdot\hat{\boldsymbol{J}} + \frac{\hbar\omega_{\text{d}}^{\text{D}}\overline{\boldsymbol{I}_1\boldsymbol{I}_2}:\overline{\boldsymbol{J}\boldsymbol{J}}}{(4\boldsymbol{J}^2-3)} - \frac{\hbar\omega_{\text{d}}^{\text{D}}(\overline{\boldsymbol{I}_1\boldsymbol{I}_1} + \overline{\boldsymbol{I}_2\boldsymbol{I}_2}):\overline{\boldsymbol{J}\boldsymbol{J}}}{4\boldsymbol{J}^2-3} \tag{15}$$

It has been shown that the last two terms give the combined dipolar/quadrupolar coupling Hamiltonian in terms of the total spin $\hat{\boldsymbol{I}}$, $-\hbar\omega_{\text{dq}}{}^{\text{D}}\overline{\boldsymbol{I}\boldsymbol{I}}:\overline{\boldsymbol{J}\boldsymbol{J}}/(4\boldsymbol{J}^2-3)$ in which

$$\omega_{\text{dq}}^{\text{D}}(para) = 2\omega_{\text{d}}^{\text{D}} - \tfrac{3}{2}\omega_{\text{q}}^{\text{D}} \tag{16}$$

$$\omega_{\text{dq}}^{\text{D}}(ortho) = \tfrac{12}{5}(\omega_{\text{d}}^{\text{D}})^2 - \tfrac{6}{5}\omega_{\text{d}}^{\text{D}}\omega_{\text{q}}^{\text{D}} + \tfrac{9}{4}(\omega_{\text{q}}^{\text{D}})^2 \tag{17}$$

The matrices $\langle \boldsymbol{\sigma}_{\text{v}}\rangle$ and $\langle \boldsymbol{\sigma}_{\text{T}}\rangle$ contain the state-to-state reorientation effective collision cross sections, averaged over a Boltzmann distribution of translational energies, associated with the irreducible first-rank tensor operator $\hat{\boldsymbol{J}}$ and the second-rank irreducible tensor operator $\overline{\boldsymbol{J}\boldsymbol{J}}/(4\boldsymbol{J}^2-3)$ respectively. The population matrix $\boldsymbol{P}$ is diagonal, with the jth element being the fractional population per state associated with the jth rotational manifold, $e^{-E_j/k_BT}/\sum_j(2j+1)e^{-E_j/k_BT}$, while $\boldsymbol{d}^{(1)}$ and $\boldsymbol{d}^{(2)}$ are vectors whose jth elements are the reduced matrix elements of $\hat{\boldsymbol{J}}$ and $\overline{\boldsymbol{J}\boldsymbol{J}}/(4\boldsymbol{J}^2-3)$ respectively, in the Edmonds convention:

$$d_j^{(1)} = \langle j|\hat{\boldsymbol{J}}|j\rangle = [j(j+1)(2j+1)]^{1/2} \tag{18}$$

$$d_j^{(2)} = \langle j|\overline{\boldsymbol{J}\boldsymbol{J}}/(4\boldsymbol{J}^2-3)|j\rangle = \frac{[j(j+1)(2j+1)]^{1/2}}{[6(2j-1)(2j+3)]^{1/2}} \tag{19}$$

These are equivalent to the equations derived by Gordon.[32,36] The correspondence with Gordon's notation is shown by Lemaire et al.[35] The cross-relaxation terms only become important at pressures below the T_1 minimum. Furthermore, with the *ortho* relaxing at least three times more slowly than the *para* D_2 and being favored in the 5:1 equilibrium ratio of these two modifications, only the relaxation of the *ortho* D_2 is observed experimentally. The equations for the relaxation behavior of D_2 are also applicable to $^{14}N_2$; however, for ^{14}N, the quadrupolar interaction dominates to the extent that the other nuclear spin interactions can be totally ignored, so that the relaxation rates for *ortho* and *para* modifications of N_2 are equal.

It has been demonstrated that the $(T_1/\rho)_{\text{lin}}$ data of H_2 and its isotopomers at infinite dilution in a rare gas are capable of distinguishing between the various proposed potential surfaces of H_2–rare gas (He, Ne, Ar).[34,35,37–39] Potential energy surfaces did not differ significantly in their ability to reproduce various experimental quantities such as virial coefficients, molecular beam scattering, transport properties and their field effects, and yet provide different results for T_1/ρ versus temperature data. The sensitivity of the computed spin relaxation times to different parts of the H_2–He potential has been examined in detail.[40] Both types of cross sections obtained from relaxation data in dilute gas are very sensitive to both the isotropic part of the potential and the $P_2(\cos\theta)$ terms, and sensitive to the $P_4(\cos\theta)$ terms, but less sensitive to higher orders. In a further example, the ^{15}N and ^{14}N spin relaxation data for N_2 in Ar have been used to distinguish between potential surfaces and to refine the best available one.[41] While quantum scattering calculations are essential for the hydrogen case, it has been shown that classical trajectory calculations are quite reliable for the case of the nitrogen molecule.

In the single relaxation time approximation (SRTA), in the extreme narrowing limit, $\boldsymbol{d}^{(1)\text{T}} \cdot \langle \boldsymbol{\sigma}_{\text{v}}\rangle^{-1} \cdot \boldsymbol{P} \cdot \boldsymbol{d}^{(1)}$ becomes $\langle j(j+1)\rangle/\sigma_{\text{J}}$, where σ_{J} [or $\mathfrak{S}'(01)$ in the literature on kinetic theory of polyatomic gases[29]] is a density-independent cross section for spin–rotation relaxation. In the same limit, $\boldsymbol{d}^{(2)\text{T}} \cdot \langle \boldsymbol{\sigma}_{\text{T}}\rangle^{-1} \cdot \boldsymbol{P} \cdot \boldsymbol{d}^{(2)}$ becomes $\frac{1}{6}\langle j(j+1)/(2j-1)(2j+3)\rangle/\sigma_{\theta,2}$, where $\sigma_{\theta,2}$ [or $\mathfrak{S}'(02)$ in the kinetic theory literature] is a density-independent cross section for molecular reorientation, the cross section associated with both dipolar and quadrupolar relaxation. This cross section differs from that for depolarized Rayleigh light scattering, σ_{DPR} (or $\mathfrak{S}_{\text{DPR}}$), only in that the latter includes contributions from a rotating collision partner, which means that $\sigma_{\theta,2}$ and σ_{DPR} are identical when the collision partner is a rare gas atom. Therefore, for a linear molecule,

$$\left(\frac{\rho}{T_1}\right)_{\text{lin,sr}} = \frac{2}{3}\frac{(\omega_{\text{sr}})^2}{L_0\langle \text{v}\rangle\sigma_{\text{J}}}\langle j(j+1)\rangle \tag{20}$$

In the 'high-temperature' or classical limit, $\langle j(j+1)\rangle = 2I_0k_{\text{B}}T$ for linear molecules, where I_0 is the molecular moment of inertia. For homonuclear dipolar relaxation,

$$\frac{\rho}{T_1} = \frac{4}{3}I_2(I_2+1)\frac{(\omega_{\text{d}})^2}{L_0\ \text{v}\ \sigma_{\theta,2}}\frac{1}{6}\ \frac{j(j+1)}{(2j\quad 1)(2j\quad 3)} \tag{21}$$

eMagRes, Online © 2007 John Wiley & Sons, Ltd.

This article was previously published in the *Encyclopedia of Magnetic Resonance* in 2007 by John Wiley & Sons, Ltd.
DOI: 10.1002/9780470034590.emrstm0185

For a quadrupolar nucleus, when the dipolar and the cross relaxation between dipolar and quadrupolar are negligible compared with the quadrupolar relaxation rate,

$$\left(\frac{\rho}{T_1}\right)_{\text{lin,q}} = \frac{(\omega_q)^2}{L_0\langle v\rangle\sigma_{\theta,2}}\frac{1}{6}\left\langle\frac{j(j+1)}{(2j-1)(2j+3)}\right\rangle \tag{22}$$

The average $\langle j(j+1)/(2j-1)(2j+3)\rangle$ goes to $\frac{1}{4}$ at the high-temperature limit, so that the above relationships, using the definitions of ω_d and ω_q, become the familiar

$$\left(\frac{\rho}{T_1}\right)_{\text{lin,d}} = \frac{1}{2}I_2(I_2+1)\frac{\gamma^4\hbar^2\langle r^{-3}\rangle^2}{L_0\langle v\rangle\sigma_{\theta,2}} \tag{23}$$

$$\left(\frac{\rho}{T_1}\right)_{\text{lin,q}} = \frac{3}{160}\frac{2I_1+3}{I_1^2(2I_1-1)}\frac{(eqQ/\hbar)^2}{L_0\langle v\rangle\sigma_{\theta,2}} \tag{24}$$

which were first derived by Gordon.[42]

In a dilute gas, the concept of a correlation time τ is physically obvious. Since a collision is itself a very short time event, the correlation time, the time it takes for a molecule to lose memory of the orientation of its angular momentum vector, is just the average time between those collisions that change the orientation of the rotational angular momentum vector:

$$\tau_J = [\rho\langle v\rangle\sigma_J]^{-1} \quad \text{or} \quad \tau_2 = [\rho\langle v\rangle\sigma_{\theta,2}]^{-1} \tag{25}$$

where σ_J and $\sigma_{\theta,2}$ are the effective cross sections for collisions that change the rotational angular momentum vector or its orientation, defined explicitly above, and can be calculated by quantum scattering or classical trajectories. The conventional definition of correlation time $\tau_{\theta,2}$ (as most often used in the liquid phase) is thus $\frac{1}{4}\tau_2$ for dipolar and quadrupolar relaxation in linear molecules in a dilute gas.[29,43,44]

Between collisions, the molecule is rotating freely. The spin–rotation interaction is not affected by the precession of the molecular symmetry axis about $\boldsymbol{J}$ between collisions. On the other hand, in dipolar relaxation, since the spin precession in the magnetic field is slow compared with molecular rotation frequencies, only the conserved or rotationally averaged component of the intramolecular dipolar magnetic field, modulated by collisions, contributes to the spin relaxation.[43] For nuclei with electric quadrupole moments, the relaxation depends on the coupling to the conserved part of the electric field gradient tensor, modulated by collisions. The averaging of second-rank tensor types of interactions leads to a factor of $\frac{1}{4}$ for linear molecules and $\frac{1}{5}$ for tetrahedral spherical tops. Similarly the symmetry axis of a symmetric top molecule precesses many times about $\boldsymbol{J}$ between collisions, thus resulting in an averaging of the spin–lattice interaction for a tensor of rank 2 by an amount $P_2(\cos\theta_0)$, where θ_0 is the angle that the dipolar axis or the electric field gradient symmetry axis makes with the molecular symmetry axis. These important and dramatic geometrical effects on the T_1/ρ values for the D spins in CD_3H, CD_2H_2, CDH_3, and CD_4 have been observed.[26] Such geometrical effects arising from averaging of the interaction during the free rotation between collisions in the gas phase do not apply to the spin–rotation mechanism, as mentioned above, so the proton relaxations in these systems have only the very small differences associated with the variation of $j(j+1)$ with rotational constants.

In the language of correlation functions, Bloom et al.[26] emphasized the physical origin of this factor of $\frac{1}{4}$ by writing the correlation time as $f_2\tau_2$, where f_2 has a different numerical value for molecules of different geometry or for different nuclear sites in the same molecule. In the language of correlation functions,

$$\tau_{\theta,2} = \int_0^\infty g(t)\,dt, \quad \text{where} \quad g(t) = [g(t)]_{\text{free rot}}[g(t)]_{\text{coll}} \tag{26}$$

$$\tau_2 = \int_0^\infty [g(t)]_{\text{coll}}\,dt, \quad f_2 = \int_0^\infty [g(t)]_{\text{free rot}}\,dt \tag{27}$$

where the oscillatory nature of the correlation function for the free rotation between collisions gives rise to the factor $f_2 = \frac{1}{4}$ for linear molecules and $\frac{1}{5}$ for tetrahedral spherical tops. For a given collision pair, for example, CH_3D–Ar, the geometrical effects on ^1H or D relaxation are different; nevertheless, the cross section $\sigma_{\theta,2}$, which is a property of the CH_3D molecule with Ar, should be the same whether derived from ^1H or D spin relaxation.

4.2 Analysis of T_1 Measurements

A review of T_1 studies in the gas phase by Armstrong[45] provides some interesting examples in the region of the T_1 minimum. The effects of centrifugal distortion can be incorporated into the T_1 expression, as was found to be necessary in the interpretation of the low-density data for proton relaxation in CH_4 and SiH_4. In the region of the T_1 minimum, the assumption of a single relaxation time for all rotational levels (SRTA) gives a poorer fit to experimental data than multiple relaxation times (MRTA). In some cases, it is found that a distribution of correlation times τ_J leads to a better fit to the data and to a more accurate spin–rotation tensor from the T_1 minimum. Beyond the T_1 minimum, T_1/ρ should be a constant independent of ρ for a given temperature. However, in some cases, dimers formed by van der Waals interactions can result in contributions to the relaxation by the rotational states of the observed molecule, as was found in H_2–Ar.[39] This leads to a maximum in the T_1/ρ versus ρ curve, which can be fitted theoretically by considering the dynamics of formation and annihilation of the dimers.

Separate relaxation of nuclei in magnetically inequivalent sites has been measured in SF_4 and in NNO. The former was carried out in the region of the T_1 minimum. The different relaxation rates are characteristic of the different paramagnetic shieldings at the two sites, which have known relationships to the respective spin–rotation tensors.[46] When measurements are made beyond the T_1 minimum in two or more nuclear sites in the molecule, the same σ_J and $\sigma_{\theta,2}$ cross sections (which are characteristic of the molecule and independent of which nucleus is observed) should result from the analysis. This was the case for NNO. Similarly, both ^1H and ^{13}C provide the same σ_J cross section for CH_4. Relaxation information for more than one nuclear site in the same molecule provides redundancy of information. Cross sections obtained from different isotopomers have different kinematic factors and should be slightly different; scattering calculations have to be carried out for each isotopomer.

eMagRes, Online © 2007 John Wiley & Sons, Ltd.

This article was previously published in the *Encyclopedia of Magnetic Resonance* in 2007 by John Wiley & Sons, Ltd.
DOI: 10.1002/9780470034590.emrstm0185

In a mixture of two gases, the analysis provides cross sections for the unlike pair of molecules if the pure gas experiment has been done, since the relaxation times in the extreme narrowing limit due to two types of collision partners are additive:[42]

$$T_1(\mathrm{A}) = (T_1/\rho)_{\mathrm{A\text{-}A}}\rho_{\mathrm{A}} + (T_1/\rho)_{\mathrm{A\text{-}B}}\rho_{\mathrm{B}} \tag{28}$$

The characteristic $(T_1/\rho)_{\mathrm{A-B}}$ provides $\sigma_J(\mathrm{A-B})$ or $\sigma_{\theta,2}(\mathrm{A-B})$.

4.3 Spin–Rotation Relaxation

In most molecules, the nuclear spin angular momentum of the ^{19}F nucleus is coupled to the molecular rotational angular momentum by a rather large spin–rotation constant, so that the ^{19}F nuclear spin is relaxed predominantly by the rotational magnetic fields. In the extreme narrowing regime, in the gas phase,

$$\left(\frac{\rho}{T_1}\right)_{\mathrm{lin.sr}} = \frac{2}{3}\frac{(\omega_{\mathrm{sr}})^2}{L_0\langle \mathrm{v}\rangle\sigma_J}\langle\, j(j+1)\rangle \tag{29}$$

where

$$(\omega_{\mathrm{sr}})^2 = C_{\mathrm{eff}}^2 = [\tfrac{1}{3}(C_\parallel + 2C_\perp)]^2 + \tfrac{4}{45}(C_\parallel - C_\perp)^2 \tag{30}$$

involving the spin–rotation tensor components, and $\langle j(j+1)\rangle = 3I_0/k_{\mathrm{B}}T$ for spherical tops such as CF_4, SiF_4, SF_6, SeF_6, and TeF_6, whereas for a linear molecule, $C_{\mathrm{eff}}^2 = C_\perp^2$ and $\langle j(j+1)\rangle = 2I_0/k_{\mathrm{B}}T$. The assumptions that allow the above T_1 equation to be used are that

1. the Larmor frequency is small compared with the collision frequency;
2. the duration of a collision is short compared with the average time between collisions;
3. the interactions among the collision partners do not significantly influence their collisions with the observed molecule;
4. bound states between the observed molecule and the collision partner have no significant effect on the spin relaxation.

Independent knowledge of the spin–rotation tensors from molecular beam electric or magnetic resonance or high-resolution microwave spectroscopy leads to $\sigma_J(T)$ directly from measurements of T_1. The temperature dependence of these cross sections appears to be described well enough by a power law:

$$\sigma_J(T) = \sigma_J(300\ \mathrm{K})(T/300\ \mathrm{K})^{-m} \tag{31}$$

These cross sections have been measured in NNO, CO_2, CO, N_2, CF_4, CH_4, SF_6, SeF_6, and TeF_6 molecules in collisions with self, Ar, Kr, Xe, N_2, CO, CO_2, HCl, CH_4, CF_4, and SF_6 molecules. Cross sections ranged from 0.09 nm^2 for SF_6 in CH_4 to 1.29 nm^2 for TeF_6 in pure TeF_6 at 300 K. The temperature exponent ranged from $m = 0.44$ for ^{13}CO in SF_6 to 1.62 for TeF_6 in SF_6, not uniformly $m = 1$ as was originally expected. Two $\sigma_J(T)$ sets for one interacting pair help to test the anisotropy of one interaction potential, offering the possibility of probing different parts of the potential surface; for example, $\sigma_J(T)$ of ^{13}CO in N_2–CO provides the anisotropy around CO, primarily $\mathrm{d}V/\mathrm{d}\theta_1$, where θ_1 is the angle that the CO molecule makes with the line connecting the centers of mass of the two molecules, and $\sigma_J(T)$ of $^{15}N_2$ in N_2–CO provides the anisotropy around N_2, primarily $\mathrm{d}V/\mathrm{d}\theta_2$, where θ_2 is the angle that the N_2 molecule makes with the intermolecular axis. A summary of σ_J cross sections and exponents m has been published.[1]

Each cross section is determined uniquely by the nature of interaction of the collision pair. As we have seen, the theoretical formalism provides the means, given the potential energy surface (PES), to calculate directly, via quantum scattering or classical trajectory methods, the observed cross sections. Nevertheless, there are interesting general observations that an examination of these cross sections reveals.[47]

1. Collision efficiencies can be defined in terms of the collision cross section divided by a geometric cross section, to take into account the relative sizes of the molecules. We have been using $(\sigma_J/\pi d_{12}{}^2)$, where d_{12} is taken from the distance scaling parameter in the conformal isotropic potential functions, the value of r at which $V = 0$. In comparing across the various observed molecules, it appears that the most important factor determining the absolute magnitude of the observed efficiencies of angular momentum change in the target molecule 1 by collision partner 2 is the anisotropy of the electronic distribution of the target molecule. For any given collision partner, the largest efficiencies are observed for the NNO molecule, followed by CO_2 and CO. To an approaching projectile, the anisotropy of the NNO molecule appears the greatest, followed by CO_2 and CO, in that order. The shape of the projectile molecule appears to be of secondary importance. Having corrected for the geometric sizes, projectiles Ar and HCl are observed to have about the same effect as do CF_4 and Xe on a nearly isotropic target such as SF_6.
2. The collision cross section for any given observed molecule increases with increasing mass (and number of electrons) of the collision partner—not unexpectedly, because of the geometric sizes. Having been corrected for the geometric sizes, the collision efficiencies also increase with increasing mass and number of electrons of the collision partner. Part of this has to do with the kinematic factors, which can be modeled by classical collisions between hard bodies, as in Chandler's perfectly rough hard spheres model.[48] The collision efficiency involves a kinematic factor containing only reduced masses and moments of inertia of the form

$$\left\{\frac{I_0(1)}{\mu_{12}d_{11}^2} + \frac{1}{2}\left[1 + \frac{I_0(1)d_{22}^2}{I_0(2)d_{11}^2}\right]\right\}^{-1} \tag{32}$$

   which applies to linear or spherical top target molecules and molecular collision partners (not rare gas atoms). The other part can be attributed to attractive forces increasing roughly with increasing number of electrons of the partner.
3. The observed collision efficiencies of the CH_4 molecule are nearly the same for nearly all partners, with the small mass of CH_4 having a leveling effect, making the reduced mass of the collision pair nearly the same for all partners.
4. Electrical moments of the collision partner enhance collision efficiencies by introducing sizable angle-dependent terms in the intermolecular potential. Thus, collision efficiencies involving HCl as a partner are higher than might be expected for its number of electrons; so do those involving CO_2 and NNO, which have large electric quadrupole moments.
5. Despite the similarities of kinematic factors for NNO with CO_2 or CO with N_2, there are clear differences in their

eMagRes, Online © 2007 John Wiley & Sons, Ltd.

This article was previously published in the *Encyclopedia of Magnetic Resonance* in 2007 by John Wiley & Sons, Ltd.
DOI: 10.1002/9780470034590.emrstm0185

Table 3 Thermal Average Cross Sections for Molecular Reorientation, $\sigma_{\theta,2}$ (300 K)[51]

	$\sigma_{\theta,2}$ (nm^2)			$\sigma_{\theta,2}/\sigma_j$		
Collision partner	$^{14}N_2$	^{14}NNO	CD_4	N_2	NNO	CD_4
CH_4 or CD_4	0.31	0.452	0.391	2.2	1.67	2.1
N_2	0.293	0.430	0.390	2.0	1.46	2.4
CO	0.32	0.470	0.381	2.1	1.42	2.4
Ar	0.32	0.474	0.354	2.1	1.26	2.5
Kr	0.41	0.656	0.459	2.3	1.18	2.5
HCl	0.36	0.634	0.536	2.0	1.22	2.3
Xe	0.44	0.762	0.520	2.2	1.18	2.3
CO_2	0.59	0.754	0.599	2.0	1.26	2.5
NNO		0.755			1.27	
CF_4	0.59	0.798	0.614	2.0	1.11	2.5
SF_6	0.73	0.994	0.779	1.9	0.96	2.3

cross sections that cannot be accounted for by the very small electric dipole moments in NNO and CO. This is an indication of the sensitivity of the σ_J cross sections to the details of the anisotropy of the intermolecular potential.

6. There is a rough correlation between the magnitude of the temperature exponent of $\sigma_J(T)$ and the well depth ε_{12} for the collision pair. This is consistent with Chandler's model,[49] in which the collision efficiencies are multiplied by an exponential factor $\exp(\varepsilon_{12}/k_B T)$ to include the effects of attractive forces.

4.4 Quadrupolar Relaxation

The ^{14}N nucleus in $^{14}N_2$ and the end ^{14}N nucleus in $^{14}N^{14}NO$ relax entirely by the quadrupolar mechanism, which allows us to characterize quadrupolar relaxation cross sections in the gas phase.[50,51] On the other hand, the much smaller electric field gradient for the middle nitrogen in NNO leads to a competing spin–rotation and quadrupolar mechanism for this nucleus. Nevertheless, $\sigma_{\theta,2}(T)$ for the $^{14}N^{14}NO$ molecule [and also $\sigma_J(T)$] should be independent of whether the end or the middle nitrogen is used to determine the cross section. Similarly, the D relaxation in CD_4 is a combination of spin–rotation and quadrupolar. Whenever more than one mechanism makes a significant contribution to the relaxation, the separation of the two leads to greater errors in the cross sections.

It has been demonstrated by McCourt and co-workers that $\sigma_J(T)$ and $\sigma_{\theta,2}(T)$ are sensitive to different parts of the anisotropic potential, thus providing independent tests. Classical trajectory calculations for $\sigma_J(T)$ and $\sigma_{\theta,2}(T)$ in the N_2–Ar system have provided agreement with the experimental values, upon refining the PES.[41] $\sigma_{\theta,2}(T)$ is found to be most sensitive to variations in the anisotropy of r_{min} of the PES, and $\sigma_J(T)$ is found to be fairly sensitive to variations both in the anisotropy of r_{min} and the angular dependence of the repulsive wall of the PES.

A summary of the results of quadrupolar relaxation in gases is given in Tables 3 and 4. A very interesting result is that for $^{14}N_2$ and $^{15}N_2$, the ratio $\sigma_{\theta,2}/\sigma_J$ is very close to 2.0, with 10 different collision partners (ranging from 1.9 to 2.3, with an average of 2.1) and m_J ranges from 0.6 to 1.0, with an average of 0.74 while $m_{\theta,2}$ ranges from 0.62 to 0.91, with an average of 0.71. On the other hand, the ratio $\sigma_{\theta,2}/\sigma_J$ for NNO is somewhat more variable, ranging from 0.96 to 1.67, with an average of 1.27, m_J ranges from 0.47 to 1.29, with an average of 0.88, and $m_{\theta,2}$ ranges from 0.66 to 0.95 with an average of 0.80. The relaxation of D in CD_4 and H in CH_4 can also be compared for 10 different collision partners, resulting in $\sigma_{\theta,2}/\sigma_J$ ranging from 2.1 to 2.5 (average 2.4), m_J ranging from 0.79 to 1.06 (average 0.88), and $m_{\theta,2}$ ranging from 0.56 to 0.75 (average 0.64).[51] Of course, the kinematic factors are slightly different for the different isotopomers, and we have already seen that kinematic factors such as moments of inertia and reduced masses play a role. In these examples, classical trajectory calculations will have to be carried out for both isotopomers in order to obtain an accurate $\sigma_{\theta,2}/\sigma_J$ ratio for each isotopomer. Other examples are $\sigma_{\theta,2}/\sigma_J = 1.38$ in pure ClF gas at 295 K[52] and $\sigma_{\theta,2}/\sigma_J = 1.6$ in pure D_2 at 293 K, increasing to very nearly 2.0 at 171 K,[53] and for CF_4 in the pure gas, the ratio is very close to 4.0, with $\sigma_{\theta,2}$ obtained from depolarized light scattering. In general, $\sigma_{\theta,2}/\sigma_J > 1.0$ has been found experimentally. Results of classical trajectory calculations with a variety of PES are generally consistent with $\sigma_{\theta,2}/\sigma_J > 1.0$. In general, $m_J > m_{\theta,2}$ has been found experimentally. The greater temperature dependence of σ_J compared with $\sigma_{\theta,2}$ is consistent with the finding by McCourt et al. that σ_J is fairly sensitive to variations in the angular dependence of the repulsive wall, whereas $\sigma_{\theta,2}$ is not, and the general observations by Gordon that σ_J contains information mainly about the higher j states, and is determined both by changes in the magnitude of the rotational angular momentum

Table 4 Temperature Dependence of Collision Cross Sections for Molecular Reorientation $\sigma_{\theta,2}(T) = \sigma_{\theta,2}(300\,\text{K})\,(T/300\,\text{K})^{-m}$

	m		
Collision partner	$^{14}N_2$	^{14}NNO	CD_4
CH_4 or CD_4	0.76	0.79	0.65
N_2	0.62	0.77	0.60
CO	0.69	0.82	0.58
Ar	0.71	0.73	0.65
Kr	0.70	0.80	0.67
HCl	0.78	0.95	0.59
Xe	0.63	0.77	0.75
CO_2	0.91	0.93	0.71
NNO		0.85	
CF_4	0.66	0.69	0.66
SF_6	0.63	0.66	0.56

eMagRes, Online © 2007 John Wiley & Sons, Ltd.

This article was previously published in the *Encyclopedia of Magnetic Resonance* in 2007 by John Wiley & Sons, Ltd.
DOI: 10.1002/9780470034590.emrstm0185

and by changes in its direction, whereas $\sigma_{\theta,2}$ are affected strongly by reorientation and only to a minor extent by changes in j.[32,41]

4.5 Intermolecular Dipole–Dipole Relaxation

In intramolecular relaxation mechanisms such as those discussed above, the interactions involved in the spin relaxation are always present within the molecule of interest; collisions interrupt molecular rotation, and thereby introduce the fluctuations of local magnetic fields or electric field gradient tensors that lead to nuclear spin relaxation. In an intermolecular mechanism, the interaction is 'on' only during a collision. By their nature, the dependence of intermolecular mechanisms on density, temperature, and magnetic field are very different from those of intramolecular mechanisms in the gas phase. It has been shown that it is possible to take advantage of such differences to separate the intermolecular mechanisms precisely from the ever-present intramolecular ones.[54–56]

In the gas phase, nuclear spin relaxation by intermolecular magnetic dipolar coupling is usually not an important mechanism. The exception is when the magnetic dipole on the collision partner is from an electron spin. The presence of the electron spin on the collision partner also generates a scalar intermolecular nuclear spin–electron spin interaction, which is responsible for the observed contact shifts discussed in Section 2.4. However, it has been shown that in the case of ^{129}Xe, this scalar mechanism[24] accounts for no more than 0.3% of the observed value of $1/T_1$ for ^{129}Xe in O_2 gas.[57] Under ideal conditions, the separation of the intermolecular dipolar from the other dominant mechanism (e.g., spin–rotation) has been quantitative, permitting the characterization of the intermolecular dipolar mechanism. This was possible for ^{1}H in CH_4, ^{19}F in CF_4, SiF_4, SF_6, SeF_6, and TeF_6 in oxygen gas.[54–56] After the spin–rotation contributions (which are proportional to $1/\rho$) were taken out, the remainder of the relaxation rate was found to be proportional to the density of oxygen for all temperatures and all fields. For example, for ^{19}F in mixtures of CF_4 in O_2, the relaxation rates ranged from 10% DD/90% SR up to 80% DD/20% SR.

There is a magnetic field dependence of the intermolecular dipolar relaxation. The duration of a collision, during which time the CF_4 and O_2 molecules are close enough for the electron spin–nuclear spin dipole interaction to cause nuclear spin transition, lasts for only a tiny fraction (1 part in 10^4) of the Larmor period of the ^{19}F nucleus, but a sizable fraction (0.04–0.2) of the Larmor period of the electron spin at typical fields 1.9–9.4 T. It has been found that a field dependence of the form

$$(1/T_1^{DD}) = (1/T_1^{DD})_0[1 - f(T)\omega_I^{1/2}] \tag{33}$$

is consistent with the experimental data for ^{129}Xe, ^{1}H in CH_4, ^{19}F in CF_4, SiF_4, SF_6, SeF_6, and TeF_6 in oxygen gas,[54–57] where $(1/T_1{}^{DD})_0$ corresponds to the zero-field limit. All these results were in the low-frequency limit; that is, the nuclear spin-bearing molecule suffers several collisions during one Larmor precession, and the duration of a collision is a fraction less than one of a Larmor cycle of the electron spin.

In the extreme narrowing limit, the correlation function approach[26] and the quantum mechanical formulation of molecular kinetic theory[27,33] both lead to

$$(1/T_1^{DD})_0 = \tfrac{16}{3} S(S+1)\gamma_I^2\gamma_S^2\frac{\hbar^2}{d^2}\left(\frac{\pi\mu}{8k_BT}\right)^{1/2} N_S \cdot F\,(V/k_BT) \tag{34}$$

where N_S is the number density of S-bearing molecules, d is the characteristic length of the intermolecular interaction, loosely referred to as the molecular diameter, and $(\pi\mu/8k_BT)^{\frac{1}{2}}$ is the reciprocal mean relative velocity $\langle v\rangle^{-1}$. The dependence of the intermolecular dipolar relaxation on the intermolecular PES is contained in $F(V/k_BT)$, which can be viewed as a measure of collision efficiency; i.e., the intermolecular dipolar relaxation rate is proportional to an *effective* collision frequency, which is a factor $F(V/k_BT)$ times that for hard spheres of diameter d at the high translational energy limit. At 300 K, $F(V/k_BT)$ is 2.04, 2.83, 3.16, 2.95, 3.66, and 3.75, respectively, for CH_4, CF_4, SiF_4, SF_6, SeF_6, and TeF_6 with O_2, and the temperature dependence is as $T^{-0.4}$. These $F(V/k_BT)$ functions are expected to serve as good tests of potential energy surfaces involving interaction with the O_2 molecule, as clearly indicated by the failure of a square well approximation to provide values of the correct order of magnitude.

The experimental results of the field dependence, obtained empirically without making any assumptions as to the form— only with the assumption that $(1/T_1{}^{DD})_0$ is field-independent— show that $f(T)$ is closely approximated by the form

$$f(T) \approx \frac{1}{24}\left(\frac{d_{eff}}{\langle v\rangle}\right)^{1/2}\left[3 + 7\left(\frac{\gamma_S}{\gamma_I}\right)^{1/2}\right] \tag{35}$$

This was arrived at by replacing the translational correlation time ($\tau_{trans} = d^2/D$ in liquid models) by the analogous characteristic time in the gas phase ($d_{eff}/\langle v\rangle$). It appears that $\pi d_{eff}{}^2 \approx \pi d^2 \cdot F(V/k_BT)$ gives a reasonable fit to the experimental field dependence. At 300 K, the values of $f(T)$ ranged from 0.0157 to 0.0243 $MHz^{-\frac{1}{2}}$ whereas the above expression leads to values of 0.0155–0.0240 $MHz^{-\frac{1}{2}}$ for CH_4, CF_4, SiF_4, and SF_6.

5 RELATED ARTICLES

Chemical Shift Scales on an Absolute Basis; Gas Phase Studies of Chemical Exchange Processes; Isotope Effects on Chemical Shifts and Coupling Constants; Relaxation: An Introduction; Relaxation Theory for Quadrupolar Nuclei; Spin–Rotation Relaxation Theory.

6 REFERENCES

1. C. J. Jameson, *Chem. Rev.*, 1991, **91**, 1375.
2. A. D. Buckingham and J. A. Pople, *Discuss. Faraday Soc.*, 1956, **22**, 17.
3. C. J. Jameson, *Bull. Magn. Reson.*, 1980, **3**, 3.
4. C. J. Jameson, A. K. Jameson, and S. M. Cohen, *J. Chem. Phys.*, 1977, **67**, 2771.

eMagRes, Online © 2007 John Wiley & Sons, Ltd.

This article was previously published in the *Encyclopedia of Magnetic Resonance* in 2007 by John Wiley & Sons, Ltd.
DOI: 10.1002/9780470034590.emrstm0185

5. F. H. A. Rummens, in *NMR Basic Principles and Progress*, eds. P. Diehl, E. Fluchs, and R. Kosfeld, Springer-Verlag, Berlin, 1975, Vol. 10, p. 1.
6. C. J. Jameson, A. K. Jameson, D. Oppusunggu, and S. Wille, *J. Chem. Phys.*, 1982, **76**, 152.
7. A. K. Jameson, C. J. Jameson, and H. S. Gutowsky, *J. Chem. Phys.*, 1970, **53**, 2310.
8. B. Bennett and W. T. Raynes, *Magn. Reson. Chem.*, 1991, **29**, 946.
9. C. J. Jameson, A. K. Jameson, and D. Oppusunggu, *J. Chem. Phys.*, 1986, **85**, 5480.
10. W. T. Raynes, A. D. Buckingham, and H. J. Bernstein, *J. Chem. Phys.*, 1962, **36**, 3481.
11. D. M. Bishop and S. M. Cybulski, *J. Magn. Reson., A*, 1994, **107**, 99.
12. C. J. Jameson and A. C. de Dios, *J. Chem. Phys.*, 1992, **97**, 417.
13. C. J. Jameson and A. C. de Dios, *J. Chem. Phys.*, 1993, **98**, 2208.
14. F. H. A. Rummens, W. T. Raynes, and H. J. Bernstein, *J. Phys. Chem.*, 1968, **72**, 2111.
15. C. J. Jameson, A. K. Jameson, and D. Oppusunggu, *J. Chem. Phys.*, 1984, **81**, 2313.
16. C. J. Jameson, A. K. Jameson, and S. M. Cohen, *J. Chem. Phys.*, 1976, **65**, 3397.
17. C. J. Jameson, A. K. Jameson, and S. M. Cohen, *Mol. Phys.*, 1975, **29**, 1919.
18. A. D. Buckingham and P. A. Kollman, *Mol. Phys.*, 1972, **23**, 65.
19. C. J. Jameson, A. K. Jameson, and S. M. Cohen, *J. Chem. Phys.*, 1973, **59**, 4540.
20. A. C. de Dios and C. J. Jameson, *Annual Reports on NMR Spectroscopy*, ed. G. A. Webb, Academic Press, London, 1994, Vol. 29, p. 1.
21. C. J. Jameson, A. K. Jameson, B. I. Baello, and H. M. Lim, *J. Chem. Phys.*, 1994, **100**, 5965.
22. C. J. Jameson, A. K. Jameson, S. Wille, and P. M. Burrell, *J. Chem. Phys.*, 1981, **74**, 853.
23. D. B. Chesnut and D. W. Wright, *J. Comput. Chem.*, 1991, **12**, 546.
24. A. Abragam, *Principles of Nuclear Magnetism*, Clarendon Press, Oxford, 1961.
25. M. Bloom and I. Oppenheim, *Adv. Chem. Phys.*, 1967, **12**, 549.
26. M. Bloom, in *MTP International Review of Science: Magnetic Resonance*, Butterworths, London, 1972, p. 505.
27. F. M. Chen and R. F. Snider, *J. Chem. Phys.*, 1967, **46**, 3937.
28. F. R. W. McCourt, T. E. Raidy, T. Rudensky, and A. C. Levi, *Can. J. Phys.*, 1975, **53**, 2463.
29. F. R. W. McCourt, J. J. M. Beenakker, W. E. Kohler, and I. Kuscer, *Nonequilibrium Phenomena in Polyatomic Gases*, Oxford University Press, Oxford, 1990, pp. 505–552.
30. C. Lemaire and R. L. Armstrong, *J. Chem. Phys.*, 1984, **81**, 1626.
31. R. G. Gordon, *Adv. Magn. Reson.*, 1968, **3**, 1.
32. W. B. Neilsen and R. G. Gordon, *J. Chem. Phys.*, 1973, **58**, **4131**, 4149.
33. B. Shizgal, *Can. J. Phys.*, 1976, **54**, 164.
34. R. L. Armstrong, M. Bogdan, K. R. Jeffrey, C. Bissonnette, and F. R. W. McCourt, *J. Chem. Phys.*, 1993, **99**, 5754.
35. C. Lemaire, R. L. Armstrong, and F. R. W. McCourt, *J. Chem. Phys.*, 1984, **81**, 5275.
36. R. G. Gordon, *J. Chem. Phys.*, 1966, **45**, 1649.
37. R. S. Wagner, R. L. Armstrong, E. C. Bissonnette, and F. R. W. McCourt, *J. Chem. Phys.*, 1990, **92**, 5907.
38. R. S. Wagner, R. L. Armstrong, C. LeMaire, and F. R. W. McCourt, *J. Chem. Phys.*, 1986, **84**, 1137.
39. C. Lemaire, R. L. Armstrong, and F. R. W. McCourt, *J. Chem. Phys.*, 1987, **87**, 6499.
40. M. J. Smith, S. Shi, H. Rabitz, and F. R. W. McCourt, *J. Chem. Phys.*, 1991, **94**, 7125.
41. L. Beneventi, P. Casavecchia, G. G. Volpi, C. C. K. Wong, and F. R. W. McCourt, *J. Chem. Phys.*, 1993, **98**, 7926.
42. R. G. Gordon, *J. Chem. Phys.*, 1966, **44**, 228.
43. R. G. Gordon, *J. Chem. Phys.*, 1966, **45**, 1635.
44. M. Bloom, F. B. Bridges, and W. N. Hardy, *Can. J. Phys.*, 1967, **45**, 3533.
45. R. L. Armstrong, *Magn. Reson. Rev.*, 1987, **12**, 91.
46. C. J. Jameson, A. K. Jameson, J. K. Hwang, and N. C. Smith, *J. Chem. Phys.*, 1988, **89**, 5642.
47. C. J. Jameson and A. K. Jameson, *J. Chem. Phys.*, 1990, **93**, 3237.
48. D. Chandler, *J. Chem. Phys.*, 1974, **60**, **3500**, 3508.
49. H. C. Andersen, D. Chandler, and J. D. Weeks, *Adv. Chem. Phys.*, 1976, **34**, 105.
50. C. J. Jameson, A. K. Jameson, and M. A. ter Horst, *J. Chem. Phys.*, 1991, **95**, 5799.
51. M. A. ter Horst, *Ph.D. Thesis, University of Illinois*, 1993.
52. K. T. Gillen, D. C. Douglass, and J. E. Griffiths, *J. Chem. Phys.*, 1978, **69**, 461.
53. M. Bogdan, K. R. Jeffrey, and R. L. Armstrong, *J. Chem. Phys.*, 1993, **98**, 6154.
54. C. J. Jameson, A. K. Jameson, J. K. Hwang, and D. Dabkowski, *J. Phys. Chem.*, 1988, **92**, 5937.
55. C. J. Jameson, A. K. Jameson, and J. K. Hwang, *J. Phys. Chem.*, 1989, **93**, 634.
56. C. J. Jameson, A. K. Jameson, and J. K. Hwang, *J. Chem. Phys.*, 1991, **94**, 172.
57. C. J. Jameson, A. K. Jameson, and J. K. Hwang, *J. Chem. Phys.*, 1988, **89**, 4074.

Biographical Sketch

Cynthia J. Jameson. *b* 1937. B.S., University of the Philippines; Ph.D., 1963, University of Illinois at Urbana-Champaign. Introduced to NMR by Herb Gutowsky. Faculty in Chemistry, University of Illinois at Chicago, 1968–present. Approx. 130 publications. Research interests include theoretical and experimental studies of the chemical shift in simple systems in the gas phase and in molecules absorbed in microporous solids, with particular emphasis on intramolecular and intermolecular shielding surfaces and averages therein; also, spin relaxation in gases and their connection with the anisotropy of intermolecular potentials and molecular dynamics.

eMagRes, Online © 2007 John Wiley & Sons, Ltd.

This article was previously published in the *Encyclopedia of Magnetic Resonance* in 2007 by John Wiley & Sons, Ltd.
DOI: 10.1002/9780470034590.emrstm0185